Research Article: Open Access

VIBGYOR ePress

International Journal of
Metallurgy and Metal Physics

Processing of Nanostructured Austempered Ductile Cast Iron (ADI) by a Novel Method

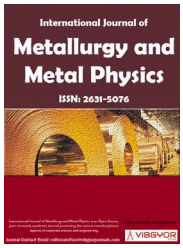

ISSN: 2631-5076

Saranya Panneerselvam and Susil K Putatunda*

Wayne State University, USA

Abstract

Austempered ductile cast iron (ADI) has emerged as a major engineering material in recent years. It has a unique microstructure consisting of bainitic ferrite and high carbon austenite. In this investigation, nanostructured austempered ductile cast iron (ADI) consisting of bainitic ferrite and high carbon austenite was developed by applying a unique process consisting of austenitization and simultaneous high temperature plastic deformation at the same austenitizing temperature followed by austempering. It was theorized by these authors that further refinement of this of ADI in the nanoscale region could possibly further enhance the mechanical properties of ADI and nanostructured ADI can be potentially a useful structured material. The influence of plastic deformation, single step and two-step austempering process on the resultant microstructure and mechanical properties of nanostructured ADI has been examined. Test results indicate that the application of high temperature plastic deformation together with austempering can result in nanostructured ADI. The extensive transmission electron microscopic investigation further confirmed the presence of nanostructured ausferritic structure in ADI as a result of the application of the unique heat treatment process.

Keywords

Austempering, Plastic deformation, Ductile cast iron, Nano-structure, Bainite, Ferrite, Austenite

Introduction

In recent years, austempered ductile cast iron (ADI) has emerged as a major engineering material for structural applications. This is due to its exceptional combination of mechanical properties such as high strength, good fracture toughness, good fatigue strength and excellent wear resistance, and good ductility. Other advantages of ADI are that, it has low production costs due to its good castability, excellent machinability and shorter heat treatment processing cycles [1,2]. ADI compares favorably with steel and aluminum castings and has been extensively used as structural components in wide range of industrial applications such as automotive, defense, agricultural, railways, mining, and construction industries.

Typical microstructure of ADI processed by conventional austempering process [3], consists of bainitic ferrite, transformed austenite enriched with carbon along with the graphite nodules. The

***Corresponding author:** *Susil K Putatunda, Department of Chemical Engineering and Materials Science, Wayne State University, 5050 Anthony Wayne Dr, Detroit, MI 48202, USA, Tel: +1-3135773808, Fax: +1-3135773810*

Accepted: October 23, 2018; **Published:** October 25, 2018

ISSN 2631-5076

Citation: Panneerselvam S, Putatunda SK (2018) Processing of Nanostructured Austempered Ductile Cast Iron (ADI) by a Novel Method. Int J Metall Met Phys 3:020

temperature and time of austempering determines the volume fraction of these phases as well as the carbon content of the austenite. As for example in ADI, lower austempering temperatures (near 260 °C) produce fine acicular ferritic structure (lower ausferrite) along with a smaller volume fraction of bainitic ferrite. This results in high tensile strength and hardness with lower ductility and poor machinability. Higher austempering temperatures (near 400 °C) produce coarser carbide free ferrite and higher volume fraction of austenite. This structure is often referred to as ausferritic structure and provides substantial improvement in ductility (with elongation of up to 14%) and good machinability. At the same time, higher austempering temperature results in relatively lower hardness and lower strength [4].

Two-step austempering process, detailed in earlier publications [5,6] involves quenching the material from the austenitizing temperature to a lower austempering temperature (to create larger supercooling to facilitate more ferrite nucleation) and heating up to a higher temperature to facilitate faster growth of carbon in austenite. Previous studies [5,6] have shown that two-step austempering process reduces the overall time for the processing of ADI and results in very fine/grain bainitic ferrite and austenitic structure and simultaneously results in significant improvement the strength and toughness of ADI compared to those processed by single step (conventional) austempering process.

While ADI has good combination of strength and toughness, refining of the micro-structures in the nanoscale range can further improve the mechanical properties and nano ADI can be a potential substitute material, in many critical structural applications, where forged or wrought high strength steels are being used.

While a significant number of nanostructured materials have been developed in recent years, the application of nanotechnology in bulk structural materials like iron and steel has been rather limited. Nano-structured grain size has been obtained in various metals and alloys by severe plastic deformation processes such as equal channel angular pressing, torsion straining, multiple forging, alloying, repetitive corrugation and straightening [7,8]. These techniques have several disadvantages because it results in defects such as microporosity, contamination and brittleness in the material. While some existing literature is available on the development of nanostructured steel and non-ferrous alloys [9], only limited investigations have been carried out to produce nanostructured ADI. Myszka, et al. [10,11] recently tried to produce Nano-structured ADI by austempering at lower bainitic transformation temperature range for a prolonged period and achieved a significant refinement of ferrite plates in less than 100 nm range. Azevedo, et al. [12] achieved refinement in austenite grain boundary by a process of rapid austenitization of prior martensitic structures. Previous studies have also detailed that the refinement of grains by transformation rather than deformation will result in improved strength and toughness. However, the characteristics of ADI including non-homogenous chemical composition, casting defects such as eutectic dendrites and porosity as well as the presence of graphite nodules makes it difficult to produce refined structure in the nanoscale range by applying only the phase transformation technique. It was theorized by these investigators that simultaneous plastic deformation of austenite grains and austempering could possibly produce grain size of ADI in the nanoscale range. During austempering process, ferrite grains nucleate at the prior austenitic grain boundaries. It was therefore hypothesized to produce nanostructured grains by elevated temperature plastic deformation of the austenite

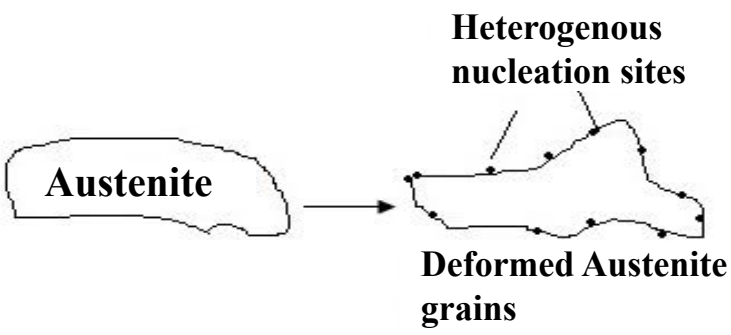

Figure 1: Deformation of austenite grain.

Table 1: Chemical composition of ductile cast iron used in this study.

Element	C	S	P	Si	Mn	Cr	Cu	Ni	Mo	Mg	V	Al
Wt%	3.44	0.008	0.016	2.46	2.46	0.05	0.52	1.03	< 0.01	0.043	0.017	0.018

grains. As the austenite grains deform, austenite grain boundaries will provide more heterogeneous nucleation sites for the growth of ferrite as shown in Figure 1. This deformed austenite, when austempered will result in extremely fine scale ferrite and austenite micro-structure in the material. This could possibly result in very fine scale ferrite and austenite most likely in the nanoscale range. Furthermore, deformation energy imparted in the material can accelerate the phase transformation reaction and thus will reduce overall process cycles for ADI.

The primary objective of this investigation was to explore the validity of this hypothesis and to examine whether nanostructured ADI can be produced by applying simultaneous plastic deformation and austempering process. The secondary objective was to characterize the microstructures and mechanical properties of nano-structured ADI.

Materials and Methods

A low alloyed ductile cast iron was used in this investigation. The chemical composition of the material is reported in Table 1. The material was cast in the form of KEEL blocks and from these cast blocks cylindrical tensile samples were prepared as per ASTM standards E-8 [13].

After fabrication, the cylindrical tensile samples were divided into 2 sets. The first set of samples was subjected to conventional single step austempering process. These were austenitized at 927 °C for 3 hours in a furnace attached to the Instron Universal Testing Machine. The samples were then plastically deformed at 927 °C (beyond its yield strength) at a strain rate of 5 mm/min, with a plastic strain of 5% by applying load prior to austempering. After deformation, the samples were transferred to a salt bath maintained at different austempering temperatures such as 288 °C, 316 °C, 360 °C and 385 °C. The samples were maintained at the specific austempering temperature for 3 hours and then air cooled to room temperature.

The second set of samples was subjected to two-step austempering process. These samples were also austenitized at 927 °C for 3 hours and then plastically deformed. The samples were then first quenched in a salt bath maintained at 260 °C, and while being kept in the salt bath for 15 minutes, the temperature of the salt bath was raised quickly to the second austempering temperatures, i.e., 288 °C, 316 °C, 360 °C and 385 °C. The samples were austempered at these temperatures for 3 hours before air cooling to room temperature.

Microstructures of the samples were examined by optical microscopy and JEOL JSM 6510 LV LGS Scanning Electron Microscopy (SEM) after polishing and etching with 3% nital solution.

Transmission Electron Microscopy analysis was carried out to confirm the presence of nanostructure in ADI and to identify the phases by indexing the diffraction patterns. Thin specimens were cut from the gauge length of the heat treated cylindrical tensile samples using a precision diamond wafering cutter. These samples were then mechanically polished to 0.1 mm thickness using a 180-grit silicon carbide paper. Final polishing was done using a cloth and 0.05 µm alumina powder solution and thickness of the samples were reduced to about 70 µm. Discs of 3 mm diameter samples were then punched from these sections. The 3 mm discs were then ion beam thinned using a dual gun ion beam milling machine, initially under 9° inclination angle and ion gun voltage of 5 kV until perforation is visible for time ranging from 3 to 5 hours depending on the initial thickness of the sample. After perforation, the ion gun voltage is reduced to 3 kV and the inclination angle is set to 6° for about 20 minutes. These samples were then examined near the perforated area using a JEOL 2010 (LaB6 Filament Gun) transmission electron microscope at an accelerating voltage of 200 kV.

X-ray diffraction (XRD) analysis was conducted using monochromatic copper K_α radiation at 30 kV and 10 mA with the Bruker Phaser II diffractometer, to estimate the volume fraction of retained austenite and its carbon content. The ferric cell sizes (d) were also determined using the well-known Scherer equation [14].

$$d = \frac{0.9\lambda}{\beta \cos\theta}$$

where λ is the wavelength, β is the breadth of

Table 2: Ferritic cell size of ADI with respect to temperature and heat treatment process.

Austempering condition	Conventional	Plastic deformation & Single-step process	Plastic deformation & Two-step process
Temperature	**Ferritic cell size**		
399 °C	27 ± 3.2	-	-
385 °C	26 ± 8.5	19.7 ± 5.6	21.8 ± 1.1
371 °C	24.3 ± 3.3	-	-
360 °C	-	19.5 ± 7.3	22.1 ± 5.0
316 °C	-	17.3 ± 5.4	18.3 ± 5.5
288 °C	19.7 ± 2.6	17.0 ± 5.7	18.4 ± 4.9
260 °C	17.5 ± 4.0	-	-

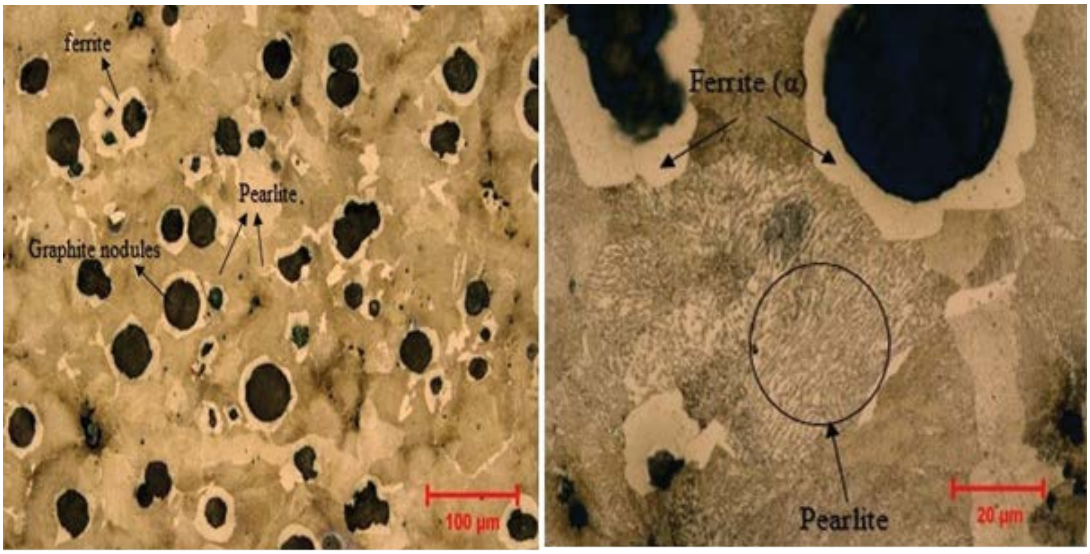

a) b)

Figure 2: As-cast microstructure of ductile cast iron. a) Optical microscope image (Mag 200x); b) Optical microscope image (Mag 1000x).

ferrite peak at half height in radians and θ is the Bragg angle.

The tensile testing of these samples was carried out on a servo-hydraulic MTS test machine as per ASTM standards E-8. Tests were carried out at constant engineering strain rate of 4×10^{-4} s^{-1}. Three to four identical test samples were tested and the yield and tensile strength were calculated from the load vs. displacement plots on a x-y recorder. The average values together with standard deviations from these samples are reported in Table 3.

Results and Discussion

Microstructure

The optical microstructure of the as cast ductile cast iron is reported in the Figure 2. The microstructure consisted of matrix of fine ferrite and pearlite along with dispersed graphite nodules. Characteristic bull's eye structure of ferrite surrounding the graphite nodules is observed. The graphite in the as-cast structure appears well rounded with 85% nodularity. Figure 3 shows the some of the optical and the high magnification SEM micrograph of the ADI samples which were austenitized, plastically deformed at 927 °C and processed by single step austempering process. The microstructure of the ADI (plastically deformed and austempered) consists of bainitic ferrite, retained austenite along with graphite nodules dispersed in the matrix. Since nucleation depends on super cooling and at lower austempering temperatures, growth rate of ferrite grains is low and it resulted finer bainitic ferrite and austenite structures at lower austempering temperatures. Thus, the lower austempering temperature of 288 °C and 316 °C resulted in finer

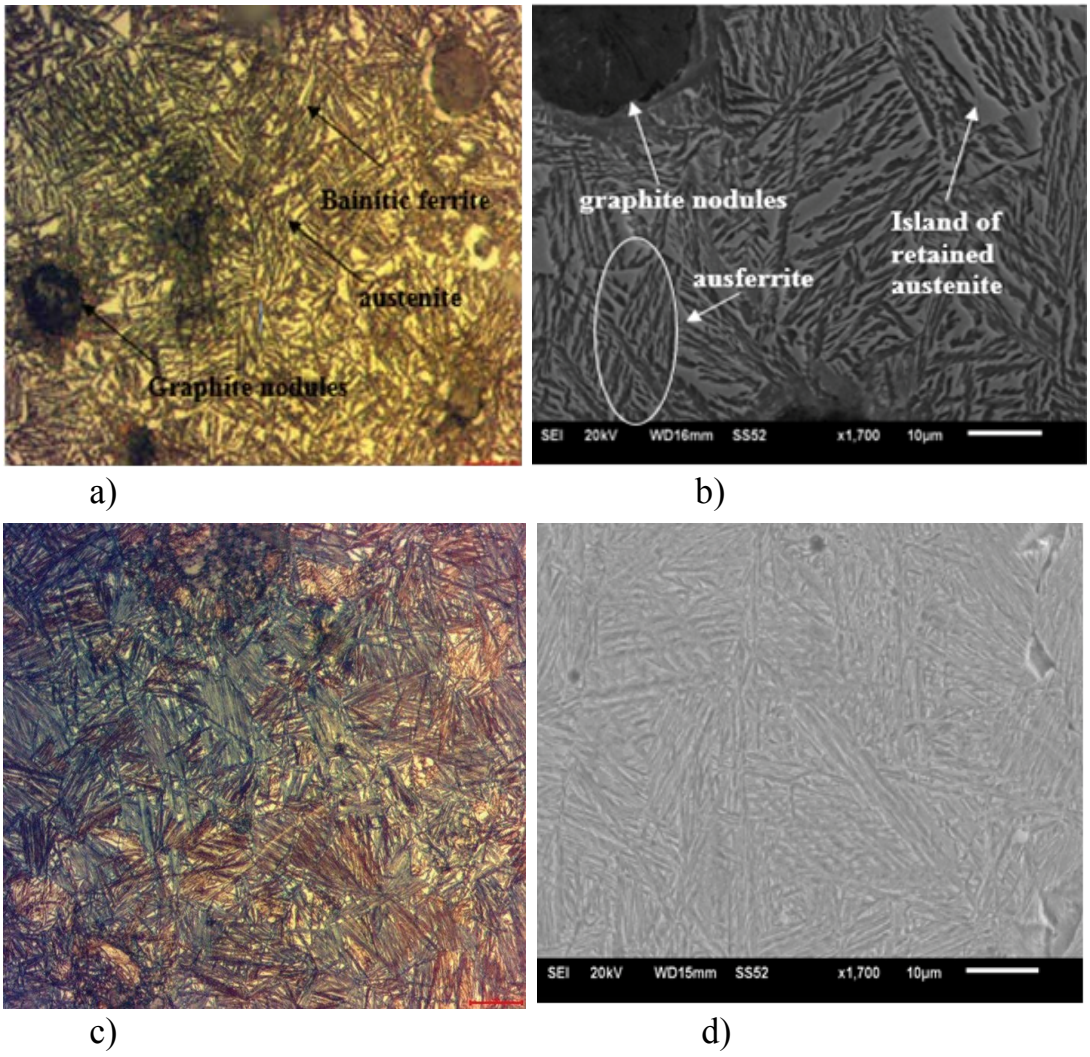

Figure 3: Typical optical and high magnification SEM micrograph of plastically deformed single step austempered ADI. a & b) Tγ = 927 °C, TPD = 927 °C, TA = 385 °C; c & d) Tγ = 927 °C, TPD = 927 °C, TA = 288 °C.

bainitic structures than those austempered at higher austempering temperatures of 360 °C and 385 °C. The coarseness of the bainitic ferrite increased with the increase in austempering temperature. The austenite was also observed in bulky or coarse at higher austempering temperatures. It was also observed that the high temperature plastic deformation did not affect the nodularity of the graphite nodule.

Figure 4 shows some of the optical and the high magnification SEM micrograph of the plastically deformed and two-step austempered samples. During plastic deformation at austenitizing temperature, the distorted austenite grain boundaries provide more heterogeneous nucleation sites for the growth of ferrite. The transformation of austenite to ferrite by the isothermal treatment occurs by nucleation and growth process. Nucleation depends on super-cooling and the high carbon content in austenite can be achieved by faster diffusion of carbon at higher austempering temperatures. Thus, once the nucleation is complete, if the ADI is heated to a higher austempering temperature, it will enable faster diffusion of carbon and thus increasing the carbon content of austenite rather quickly. During the two-step austempering process, the ductile cast iron samples were initially quenched to a lower temperature of 260 °C which facilitates higher super cooling and hence greater ferrite nucleation. As the austempering temperature was raised to the second austempering temperature, the faster growth of the already nucleated ferrite occurs alongside faster diffusion of carbon to austenite. Lower austempering temperature of 288 °C and 316 °C resulted in finer ferritic structures than those austempered at higher austempering temperatures of 360 °C and 385 °C. The

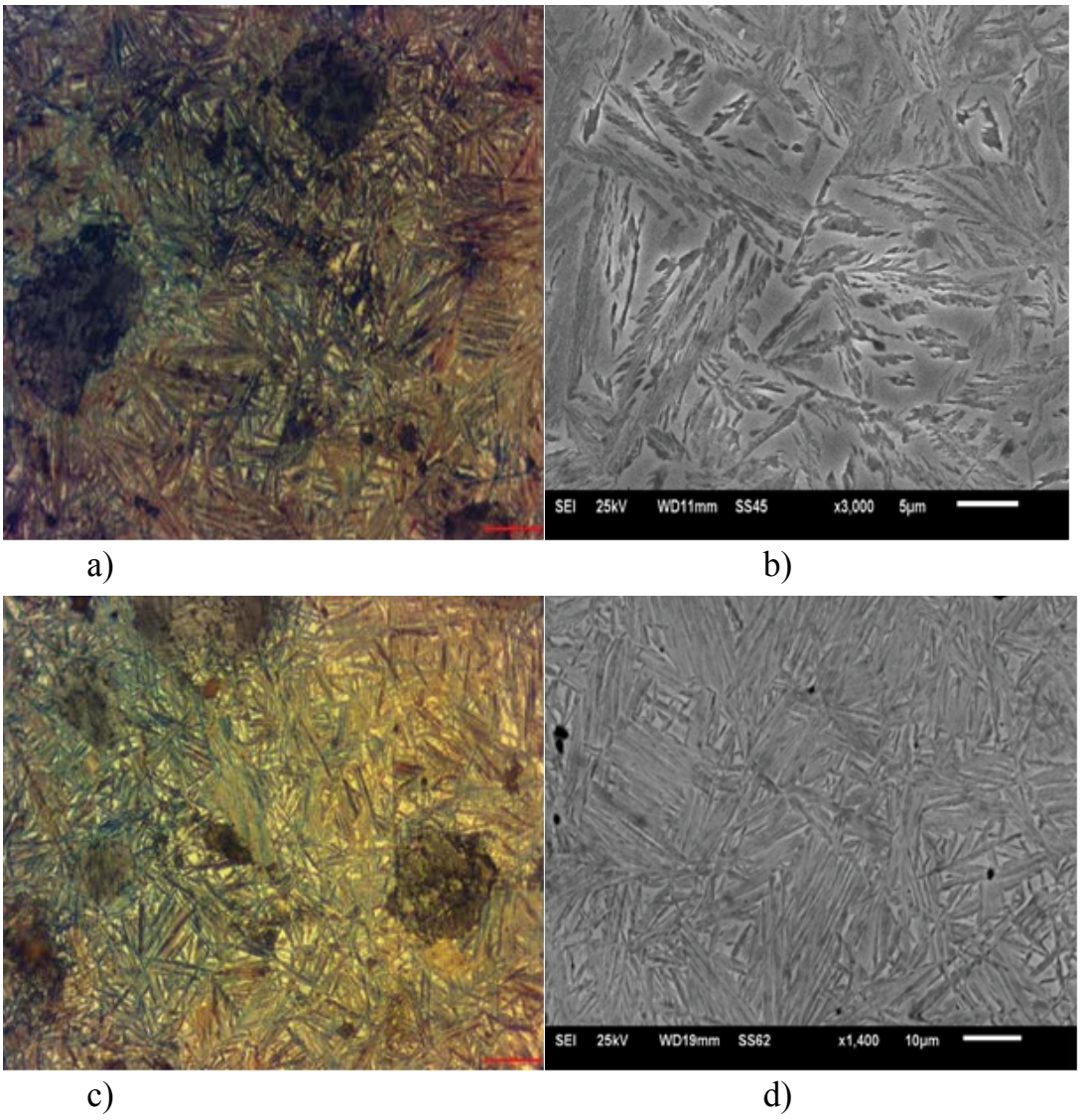

Figure 4: Typical optical and high magnification SEM micrograph of plastically deformed, two step austempered ADI. a & b) Tγ = 927 °C, TPD = 927 °C, TA1 = 260 °C, TA2 = 385 °C; c & d) Tγ = 927 °C, TPD = 927 °C, TA1 = 260 °C, TA2 = 288 °C.

nodularity of the graphite was also not affected by in two step process.

The volume fraction of the austenite, determined from the X-ray diffraction analysis is shown in the Figure 5. The average volume fraction of austenite was observed to increase as the austempering temperature is increased. It is also evident from the Figure 5 that the high temperature plastic deformation along with two-step austempering process has resulted in a higher volume fraction of austenite than the single step austempering process. During the two-step austempering process, the ductile cast iron samples were initially quenched to a lower temperature of 260 °C which facilitates higher super cooling and hence greater ferrite nucleation. More ferrite particles are nucleated in this case but the growth rate of ferrite was low because of lower average temperature in these samples. Therefore, two step austempered ADI had higher volume fraction of austenite, at the same time finer ausferritic structure. Thus, it appears that nucleation process is more dominant than the growth process in ADI. Comparatively, the volume fraction of ferrite the high temperature plastically deformed ADI samples is significantly lower than the conventional single step austempered ADI detailed in our previous investigation [4]. Thus, this unique process will result in finer ferrite and austenite together with larger volume fraction of austenite in the material. This is expected to result in further improvement in mechanical properties in ADI as compared to conventionally austempered samples

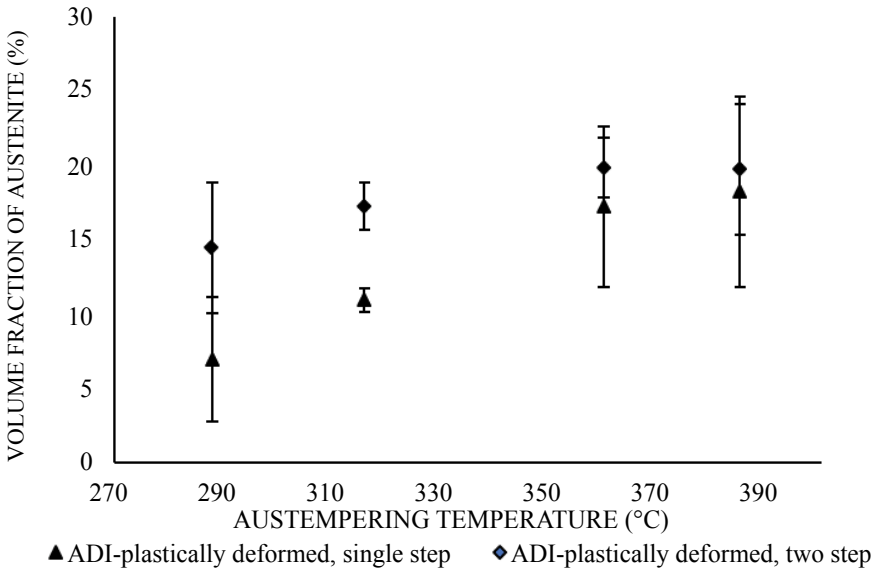

Figure 5: Influence of high temperature plastic deformation on the volume fraction of transformed austenite with respect to single step and two step austempering.

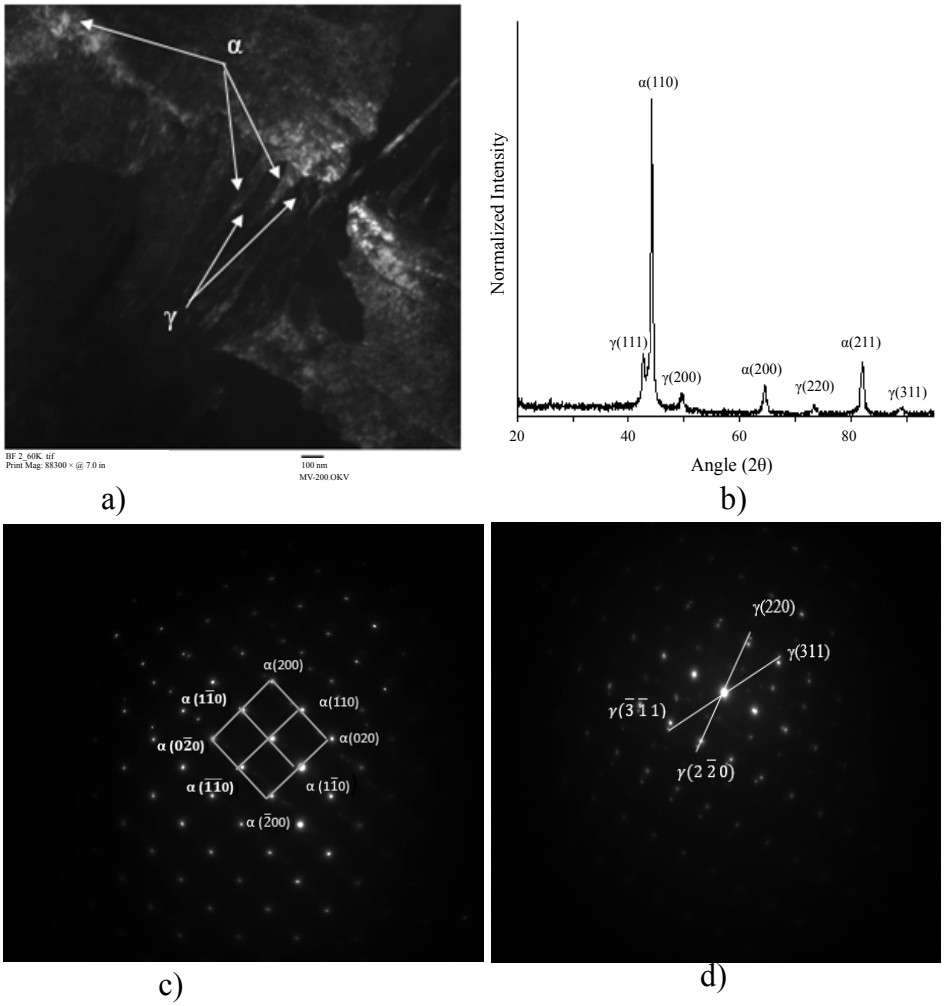

Figure 6: TEM micrographs of ductile cast iron conventionally austempered at 385 °C. a) Dark field image from α (110) bainitic ferrite reflection; b) X-ray diffraction profile; c) SAED pattern for bainitic ferrite phase; d) SAED pattern for austenite.

by single step process.

The ferritic cell size (d) was determined for all the heat treated ADI samples using the well-known Scherer equation [14]. It is the average size of the crystallite or ferritic laths, which is smaller than the grain size. Average ferritic cell size is also the measure of the mean free path for the dislocation motion in the material. Table 2 reports the effect of austempering temperatures on the ferritic cell sizes of the plastically deformed ADI samples. The average ferritic cell size of the ADI increases with the increase in austempering temperature. Statistically, no significant difference was observed in the ferritic cell sizes between the single step and two step processing in the plastically deformed ADI. Plastic deformation has significantly reduced the ferritic cell size when compared with in conventional ADI as reported in our previous investigation [15]. These data from Figure 6 confirms that nanostructured ADI can be produced by our unique process.

The carbon content of austenite (Cγ) at the austenizing temperature is given by equation [16]:

$$C_o = \frac{T\gamma}{420} - 0.17 \times (\%\, Si) - 0.95$$

Using the above equation, for our present material C_o comes to be around 0.65. This carbon will be distributed in the transformed ferrite (α) and transformed austenitic in the material. Thus, we can express C_o as:

$$C_o = X_\alpha . C_\alpha + X_\gamma . C_\gamma$$

Where C_α is the carbon content of ferrite and Cγ is the carbon content of austenite, X_α and Xγ are the volume fraction of austenite respectively. Since, ferrite dissolves very little carbon C_α ~ very small. Therefore, the term $X_\alpha.C_\alpha$ can be ignored and C_o can be approximated to Xγ.Cγ. This equation in-

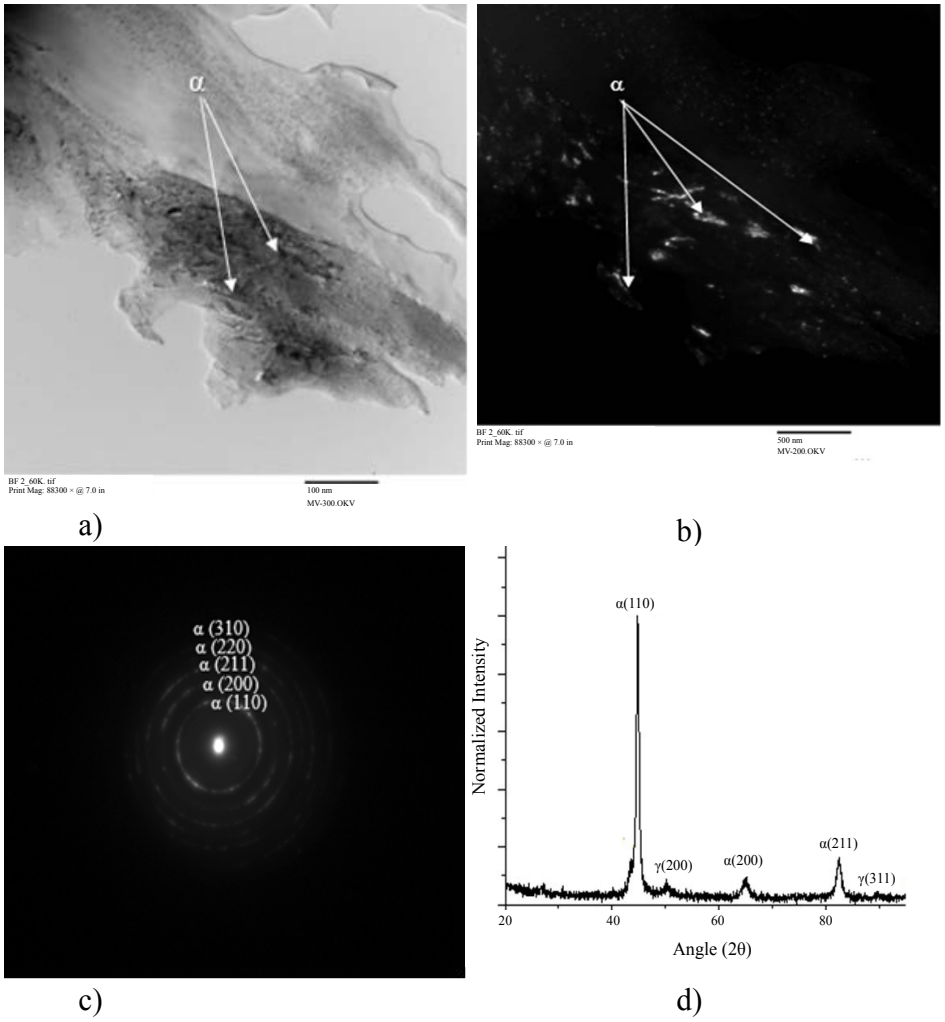

Figure 7: TEM micrographs of ADI sample austenitized and plastically deformed at 927 °C and austempered at 385 °C. a) Bright filed image; b) Dark field image from α (110) bainitic ferrite reflection; c) Ring SAED pattern for bainitic ferrite phase; d) X-ray diffraction profile.

dicates as volume fraction of austenite increases the carbon content should decrease. Since, the two step austempered samples had lower volume fraction of austenite, the carbon content was higher in these samples.

The typical dark field image TEM micrograph of the conventionally austempered ductile cast iron without plastic deformation is shown in Figure 6a. The dark field image obtained from the α (110) bainitic ferrite reflection shows the coarse bainitic ferrites and retained austenite present in between the bainitic ferrite laths. This is in good agreement with the X-ray diffraction profile of the conventionally austempered ductile cast iron (ADI) showing the presence of both the ferrite and austenite phases as shown in the Figure 6b. The SAED pattern obtained shows the typical spot diffraction pattern with well-defined spacing and angles in the Figure 6c and Figure 6d and confirms the presence of bainitic ferrite and austenite phases respectively. Figure 7a shows the TEM bright field of the ADI sample, austenitized and plastically deformed at 927 °C and processed by single step austempering at 385 °C. The dark field image as shown in Figure 7b obtained using the bainitic ferrite reflection α (110) shows the bainitic ferrite structure which occurs as tiny subunits. Similar observation is obtained for the austenite reflection. The corresponding X-ray diffraction pattern shown in the Figure 7d confirms the presence of austenite and ferrite phases in the plastically deformed ADI. In the X-ray diffraction profile, the γ (111) is not prominent and the γ (220) peak is not present indicating the lower volume fraction of austenite in these plastically deformed samples. Figure 8 shows TEM bright field and dark field images of the ADI samples, austenitized and plastically deformed at 927 °C and processed by two-step austempering process. The bright field image in Figure 8a shows the bainitic ferrite subunits with austenite laths in between them in the nanoscale range. The bainitic ferrite appears as very fine subunits with the films

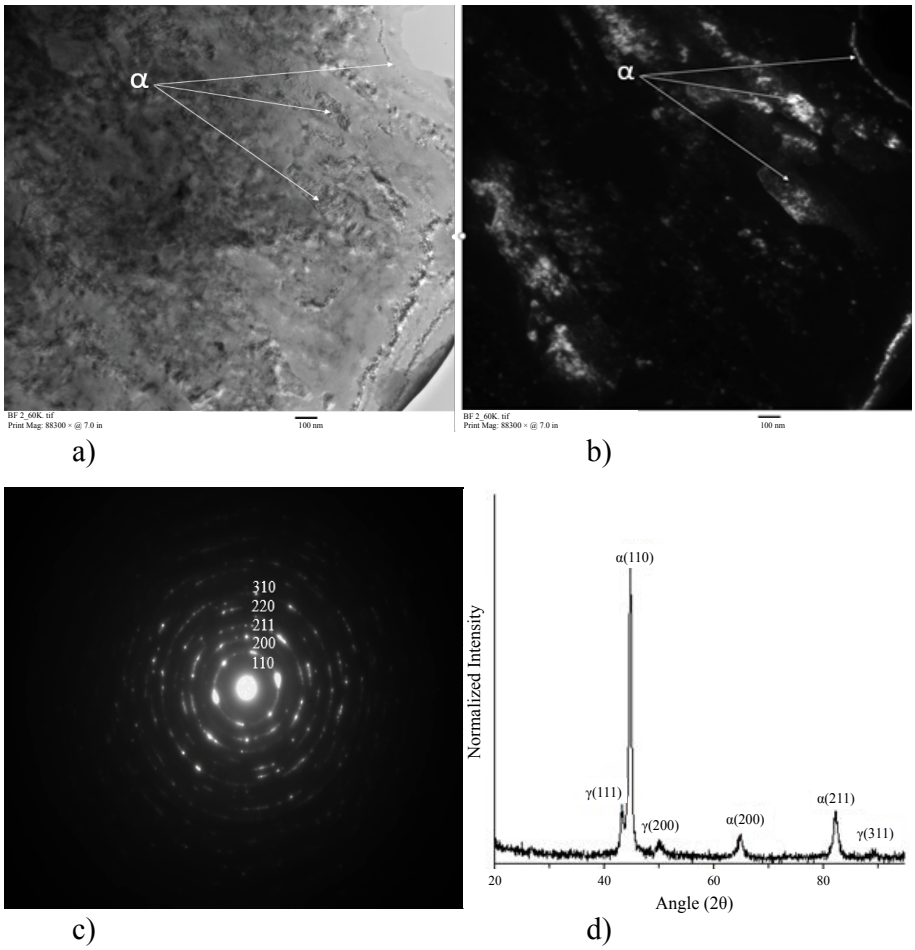

Figure 8: TEM micrographs of ADI sample austenitized and plastically deformed at 927 °C and two-step austempered at T_{A1} = 260 °C, T_{A2} = 385 °C. a) Bright filed image; b) Dark field image from α (110) bainitic ferrite reflection; c) Ring SAED pattern for bainitic ferrite phase; d) X-ray diffraction profile.

of austenite between them. The X-ray diffraction profile in Figure 8d of the plastically deformed, two step austempered ADI show faint austenite peaks, indicating the lesser volume fraction of austenite in these samples, when compared to conventional ADI. Only γ (220) peak is not present in these samples.

The selected area electron diffraction (SAED) pattern of these samples in Figure 7c and Figure 8c showed continuous rings for bainitic ferrite and austenite. This continuous ring arises from the ultra-fine grain structures. The diffraction pattern changes from spot to rings (example: Figure 6c and Figure 7c) when the refinement of the grains occurs [17] as shown in the Figure 9. The refinement of the grain has resulted in the refinement of the crystallites inside the grains. Thus, the plastic deformation of the ADI resulted in ultra-fine nanocrystalline bainitic ferrite and austenite as evident from the TEM micrograph and SAED pattern.

Table 3 reports the mechanical properties of the (plastically deformed) ADI and austempered by single step and two step austempering processes.

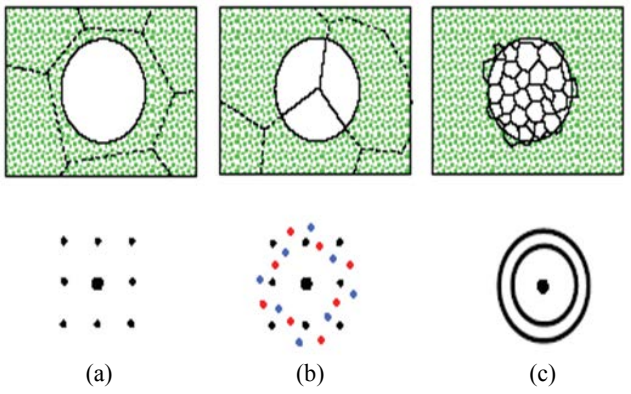

Figure 9: Changes in diffraction pattern with respect to grain size [17].

Plastic deformation was performed at the strain rate of 5 mm/min. The samples underwent plastic strain of 5% at the austenitizing temperature prior to austempering. These results show that the ADI samples austempered at lower austempering temperatures had higher strength and hardness. A difference of 39% in the yield strength and approximately 22% for the ultimate tensile strength was observed between the upper and lower austempering temperatures for the samples austempered by single step austempering process. This can be attributed to the presence of finer nanostructured bainitic ferrite and austenitic structure in the samples austempered at lower austempering temperatures. As mentioned earlier, at higher austempering temperatures of 360 °C and 385 °C coarser and feathery ferrite along with higher volume fraction of islands of austenite was observed. This micro-structural feature is responsible for the lower strength in these ADI samples. Two step austempered samples had higher strength than the single step austempered samples even though the average bainitic ferrite grains were larger in these samples. However, no significant difference in the hardness value was observed. In two-step austempered samples, larger volume fraction of carbon stabilized austenite resulted in higher strength than the ADI samples processed by single step austempering process.

Conclusions

1. In this investigation, nanostructured ADI was produced by a unique heat treatment process conceived by these investigators. This process involves high temperature plastic deformation during austenitization followed by either single or two-step austempering process.
2. High temperature plastic deformation and aus-

Table 3: The mechanical properties of plastically deformed ADI with respect to heat treatment. (ADI samples austenitized at 927 °C, plastically deformed, followed by either single step/two - step austempering).

Austempering condition	Austempering temperature (°C)	Yield strength (MPa)	Ultimate tensile strength (MPa)	Hardness (HRC)
Single step process	385	709 ± 14	970 ± 24	35 ± 3
	360	750 ± 30	1109 ± 67	37 ± 3
	316	896 ± 6	971 ± 18	48 ± 8
	288	1159 ± 35	1244 ± 42	49 ± 5
Two-step process	385	953 ± 22	1065 ± 29	34 ± 2
	360	963 ± 15	1093 ± 52	37 ± 2
	316	1199 ± 26	1334 ± 38	41 ± 2
	288	1208 ± 18	1304 ± 22	42 ± 2

tempering in the lower bainitic temperature range resulted in ultra-fine laths of bainitic ferrite and retained austenite in ADI.

3. The width of the bainitic ferrite increased with the increase in austempering temperature. High temperature plastic deformation greatly reduced the width of bainitic ferrite in the ADI samples austempered in the upper bainitic temperatures when compared to conventionally processed ADI.
4. Plastic deformation resulted in the grain refinement in the nanoscale range which is evident from the ring SAED pattern obtained from the plastically deformed ADI samples.
5. The proposed unique heat treatment process involving a combination of high temperature plastic deformation and subsequent austempering has resulted in a robust process window that makes nano ADI with better mechanical properties, practically possible from production standpoint.
6. While these investigators were successful to produce Nano-structured ADI, we have not been able to optimize the process parameters. Further investigations are necessary to find the optimum percentage of typo plastic deformation, austenitizing temperature, austempering time and temperature so that nano ADI with exceptional combination of strength, toughness and ductility can be produced.

References

1. Sellamuthu P, Harris Samuel DG, Dinakaran D, Premkumar VP, Li Z, et al. (2018) Austempered Ductile Iron (ADI): Influence of austempering temperature on microstructure, mechanical and wear properties and energy consumption. Metals 8: 53.
2. Fatahalla N, Hussein O (2015) Microstructure, mechanical properties, toughness, wear characteristics and fracture phenomena of austenitized and austempered low-alloyed ductile iron. Open Access Libr J 2: 1-16.
3. Janowak JF, Gundlach RB, Eldis GT, Rohrting K (1982) Technical advances in cast iron metallurgy. International Cast Metal Journal 6: 28-42.
4. Panneerselvam S, Martis C, Putatunda SK, Boileau J (2015) An investigation on the stability of austenite in austempered ductile cast iron (ADI). Materials Science and Engineering A 626: 237-246.
5. Putatunda SK (2001) Development of austempered ductile cast iron (ADI) with simultaneous high yield strength and fracture toughness by a novel two-step austempering process. Materials Science and Engineering A 315: 70-80.
6. Yang J, Putatunda SK (2004) Improvement in strength and toughness of austempered ductile cast iron by a novel two-step austempering process. Materials and Design 25: 219-230.
7. Valiev RZ, Langdon TG (2006) Principles of equal-channel angular pressing as a processing tool for grain refinement. Progress in Materials Science 51: 881-981.
8. Hurley PJ, Hodgson PD, Muddle BC (1999) Analysis and characterization of ultra-fine ferrite produced during a new steel strip rolling process. Scripta Materialia 40: 433-438.
9. Bhadeshia HKDH (2013) The first nanostructured metal. Science and Technology of Advanced Materials 14: 014202.
10. Myszka D, Skołek E, Wieczorek A (2014) Manufacture of toothed elements in nanoausferritic ductile iron. Archives of Metallurgy and Materials 59: 1217-1221.
11. Myszka D, Wasiluk K, Skoek E, Swiatnicki W (2015) Nanoausferritic matrix of ductile iron. Materials Science and Technology 31: 829-834.
12. Azevedo CRF, Garboggini AA, Tschipitschin AP (1993) Effect of austenite grain refinement on morphology of product of bainitic reaction in austempered ductile iron. Materials Science and Technology 9: 705-710.
13. (2016) ASTM E8/E8M-16a: Standard test methods for tension testing of metallic materials. ASTM International.
14. Cullity BD, Stock SR (2001) Elements of X-ray diffraction. (3rd edn), Prentice Hall.
15. Yang J, Putatunda SK (2004) Influence of a novel two-step austempering process on the strain-hardening behavior of austempered ductile cast iron (ADI). Materials Science and Engineering A 382: 265-279.
16. RC Voigt, CR Loper (1984) Austempered ductile iron process control and quality assurance. Journal of Heat Treating 3: 291-309.
17. Asadabad MA, Eskandari MJ (2016) Electron diffraction. Modern Electron Microscopy in Physical and Life Sciences 3-24.

ISSN 2631-5076